Alcohol Partition in a Water-in-Oil Microemulsion: Small-Angle Neutron-Scattering Contrast Measurements

A. L. Compere, W. L. Griffith, and J. S. Johnson, Jr.*

Chemical and Analytical Sciences Division, Oak Ridge National Laboratory, Oak Ridge, Tennessee 37831-6201

E. Caponetti, D. Chillura-Martino, and R. Triolo

Dipartimento Chimica Fisica, via Archirafi 26, 91023 Palermo, Italy

Received: January 29, 1997; In Final Form: June 19, 1997[⊗]

We have earlier reported estimates of alcohol distribution between a water-in-oil microemulsion and the continuous hydrocarbon phase, based on the core surface area, the dimensions being determined by small-angle neutron scattering from the microemulsions with D_2O cores. To make a more direct determination, we have carried out contrast measurements on three of the compositions with other components, except for the surfactant, potassium oleate, deuterated: water, hexadecane, and the alcohol 1-heptanol or 1-octanol. Patterns were obtained with individual components isotopically labeled and with combinations of components labeled. Of the models tested, oblate ellipsoids gave better fits to all contrasts for a given composition than prolate ellipsoids or polydisperse spheres. The parameters were also more plausible. A somewhat higher proportion of alcohol was found to be distributed in the particles than earlier estimated from surface-area arguments.

Introduction

We previously reported estimates of alcohol distribution in a water-in-oil microemulsion, based on filling the area of the interface between the water core and the surfactant/cosurfactant shell with the headgroups.[1] The dimensions required were obtained by small-angle neutron scattering (SANS). The systems studied were comprised of potassium oleate, hexadecane, D_2O, and different amounts of one of the alcohols 1-pentanol, 1-hexanol, 1-heptanol, and 1-octanol. Two regions of the phase diagram were studied: in one, there were 45 mol of water and 15 mol of hydrocarbon per mole of potassium oleate; in the other, there were 30 mol of water and 5.5 mol of hydrocarbon per mole surfactant. The range of alcohols added covered most of the one-phase region for the two compositions.

The SANS patterns were interpreted on the basis of an oblate-ellipsoidal model we have used in a number of studies of w/o microemulsions prepared from these and similar components.[2−5] In estimating the alcohols in the particles, 60 Å^2 was assigned to each of the surfactant carboxylates, and the remaining core area divided by 20 Å^2, the assumed area of alcoholic headgroups.

The alcohol distributions and their trends with composition obtained in this way were plausible. However, questions can be raised about the bases of the analysis. The alcohol area, from a compilation in the literature,[6] comes mainly from Langmuir-balance measurements of surface area and is probably a fairly good approximation. The carboxylate area is less established; it was estimated[1] from oil/water micelles for fatty acids and from water/oil microemulsions of surfactants having other headgroups. There is also not general agreement about the model used. Oblate ellipsoids have for the w/o systems we have investigated usually given better fits and more credible parameters than other models tried, for example, prolate ellipsoids or polydisperse spheres. However, with only D_2O contrasts, the distinction between models is not always great, and others have preferred alternative interpretations for w/o microemulsions; polydispersity is frequently invoked to deal with the absence of fine structure, predicted in computations for monodisperse spheres, in the experimental patterns.

Further evidence is desirable. An obvious route is to take further advantage of the large differences of hydrogen and deuterium in cross sections for coherent neutron scattering, by measuring patterns for the same chemical compositions, but with hydrocarbon and alcohol isotopically labeled. Trying to fit all patterns provides a more definitive test of models and a more direct estimation of alcohol distribution. We report here extended contrast patterns for three of the compositions in ref 1, one with octanol and two with heptanol.

Experimental Section

SANS. Patterns were measured on the 30-m (maximum, source to detector) SANS diffractometer at the High-Flux Isotope Reactor of Oak Ridge National Laboratory. The neutron wavelength (λ) was 4.75 Å. The solutions were contained in quartz spectrophotometer cells of 1 mm solution path lengths. Temperatures were maintained by fluid circulation from external baths. The sample-to-detector distances ranged from 1.5 to 19 m, as needed to obtain the range of Q ($=(4\pi/\lambda)\sin\theta$, 2θ being the scattering angle) reported.

Scattering from samples was corrected for detector background, empty cell scattering, sample transmission, and detector sensitivity. Radial averages were obtained from two-dimensional scattering patterns and runs at different distances were combined, with programs developed for the diffractometer. Absolute intensities, reported as differential cross-section densities with angle, $d\Sigma(Q)/d\Omega$ (cm^2/cm^3, or cm^{-1}), were based on the standards provided at the diffractometer; the calibrations are estimated to be good to ±15%.

Materials. Potassium oleate was obtained as described in ref 2. D_2O was from Aldrich Chemical, and was assumed to contain 1% H. The hydrogen form of *n*-hexadecane was from Aldrich, and 1-heptanol and 1-octanol were Fisher certified reagents. Deuterated organic compounds were from Cambridge Isotope Laboratories. In the octanol series, hexadecane-d_{34} was stated to be 96% D, and in the heptanol contrasts, 99% D. The

[⊗] Abstract published in *Advance ACS Abstracts,* August 1, 1997.

S1089-5647(97)00363-5 CCC: $14.00

TABLE 1: Stoichiometries in Contrast Measurements of Alcohol Distribution (Moles of Component/Mole Potassium Oleate)

	Deuterated Components				
	D_2O	$C_{16}D_{34}$	D_2O/ $C_{16}D_{34}$	$C_8D_{17}OH$ or $C_7D_{15}OH$	$D_2O/C_{16}D_{34}$/ $C_8D_{17}OH$ or $C_7D_{15}OH$
MOLES					
			C8c		
KOleate	1	1	1	1	1
H_2O		44.89		45.22	
D_2O	44.66		45.88		45.57
$C_{16}H_{34}$	14.95			14.91	
$C_{16}D_{34}$		15.00	15.20		15.21
$C_8H_{17}OH$	5.463	5.450	5.480		
$C_8D_{17}OH$				5.546	5.490
			C7c		
KOleate	1	1	1	1	1
H_2O		45.01		45.21	
D_2O	45.39		44.57		45.12
$C_{16}H_{34}$	15.05			15.1	
$C_{16}D_{34}$		14.89	14.83		14.89
$C_7H_{15}OH$	7.231	7.176	7.160		
$C_7D_{15}OH$				7.248	7.180
			C7C		
KOleate	1	1	1	1	1
H_2O		30.66		30.54	
D_2O	30.30		29.77		29.94
$C_{16}H_{34}$	5.516			5.537	
$C_{16}D_{34}$		5.483	5.495		5.523
$C_7H_{15}OH$	7.231	7.159	7.185		
$C_7D_{15}OH$				7.218	7.263

hydroxyl groups of the alcohols were −OH, rather than −OD. Octanol-d_{17} was stated to be 98% D, and heptanol-d_{15}, 99% D. Allowances for the minor departures from isotope purities were made in the computation of scattering-length densities in the programs. Hydrogen and deuterium of water and of the alcohol −OH group are exchangeable, and the water and alcoholic headgroup scattering lengths were computed from the average of the exchangeable H and D of the composition.

Owing to the cost of deuterated chemicals, the samples were prepared only in the volume necessary to fill the cells, less than 0.4 mL. Determination of composition was by weight. The stoichiometries are given in Table 1.

Volumes and scattering lengths. The group volumes used were for the most part the same as in the previously cited papers: 32.7 mL/mol for methyl; 16.2 mL/mol for methylene; 12.4 mL/mol for −CH═; 10.3 mL/mol for alcoholic −OH; and 3.6 mL/mol for K^+. For the carboxylate group, however, we used here a somewhat different value, 20.7 mL/mol, based mainly on the arguments of Høiland;[7] this choice was discussed in ref 8. Scattering lengths were taken from a standard compilation.[9]

Results

SANS Patterns. Three compositions (Table 1) were selected from the sets in ref 1 for contrast measurements: C8c (octanol) and C7c (heptanol) are of relatively low volume fraction microemulsion components, but of relatively high water/surfactant ratio, the alcohol content being in the midrange of the respective sets; C7C (heptanol) is of relatively high volume fraction disperse phase, but lower water/surfactant ratio, and also in midrange of its series with respect to alcohol content. In general, particle sizes increase with water/surfactant ratio. Three contrasts were carried out with the single components water, hexadecane, or alcohol deuterated. One had both water and hydrocarbon deuterated, and another all components except potassium oleate deuterated. None of these compositions gave

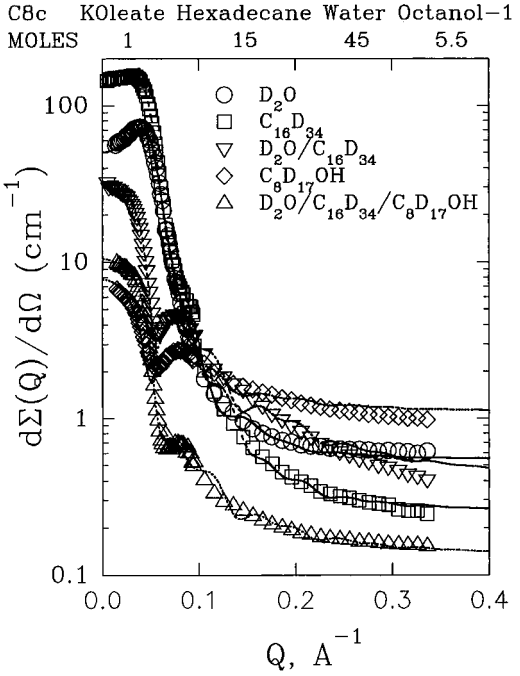

Figure 1. Oblate ellipsoidal model, C8c. Symbols, experimental points, indicate deuterated components. Parameters of computed curves in Table 2.

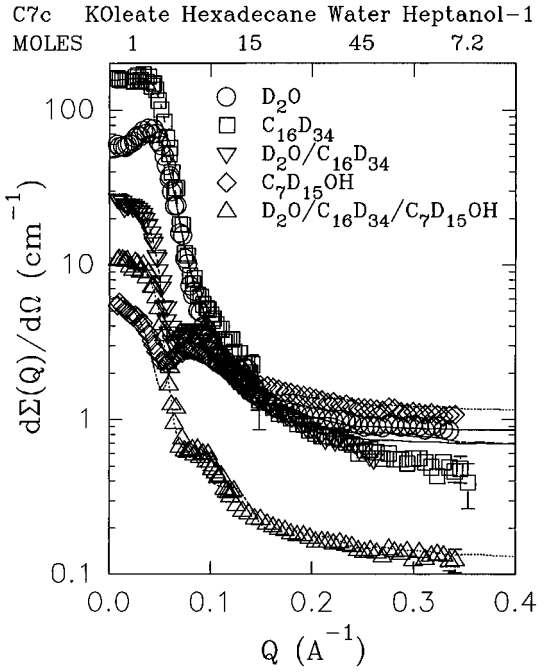

Figure 2. Oblate ellipsoidal model, C7c. Symbols, experimental points, indicate deuterated components. Parameters of computed curves in Table 2.

indications of proximity to critical points, as some of the pentanol-containing systems did.

The SANS patterns of C8c are presented as the points in Figure 1, of C7c, in Figure 2, and of C7C, in Figure 3. The symbols identify the components deuterated. As expected, the patterns for the various contrasts of the same composition are very different, both in absolute intensity and in shape. With D_2O and $C_{16}D_{34}$, in which the contrasts are primarily between the core or total particle and continuous phase, a peak occurs at low Q, from interparticle scattering. For the other compositions, in which contrast between shells vs core and continuous phase are important, a minimum in intensity, or an inflection

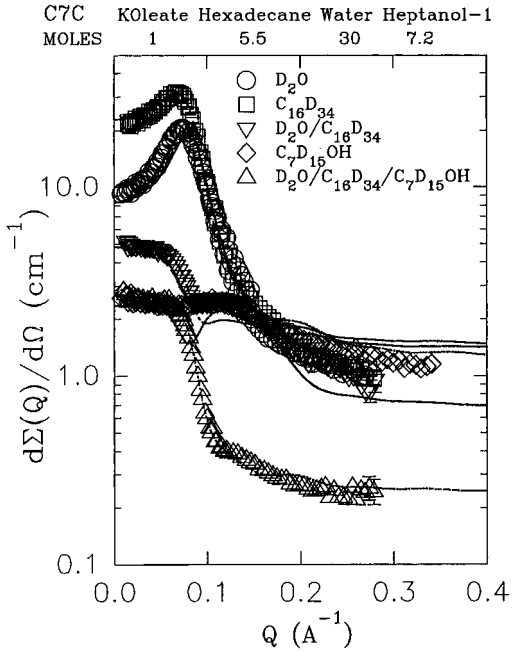

Figure 3. Oblate ellipsoidal model, C7C. Symbols, experimental points, indicate deuterated components. Parameters of computed curves in Table 2.

indicating one, occurs in the patterns. The problem is to find a model that approximates all of the contrasts of a given composition.

Models. *General.* The equations used to compute patterns for the various models are embedded in various computer programs developed over time and will be incorporated here mainly by reference, because they are too cumbersome to be repeated in detail. For the reader unfamiliar with the subject, the following qualitative discussion may be helpful in defining terms.

In absence of correlation between interparticle separation and particle size and/or particle orientation, the (coherent) scattered neutron intensity from a collection of particles dispersed in a continuous medium, $I(Q)$, is given by the following equation:

$$I(Q) = N_p[\langle F(Q)\rangle^2 S(Q) + \langle F(Q)^2\rangle - \langle F(Q)\rangle^2]$$

where N_p is the number particle density in droplets/cm^3; $F(Q) = \Sigma_j b_j \exp(i\mathbf{Q}\mathbf{r}_j)$ is the scattering amplitude of a collection of atoms of scattering length b_j, whose position relative to an arbitrary origin is defined by the vector $\mathbf{r}_j$ (the sum is over the atoms in the particle, and this expression, given for illustrative purposes, refers to a vacuum as the continuous phase; the contrast with the continuous medium is included in the computation of patterns here); the brackets $\langle\ \rangle$, denote the time-averaged value; and $S(Q)$, known as the interparticle structure function, is the Fourier transform of the particle−particle correlation function $h_{ij}(r) + 1$, which measures the probability of finding a particle j at a distance r from a particle i centered at the origin. For monodisperse spheres, where $\langle F(Q)\rangle^2 = \langle F(Q)^2\rangle$, $F(Q)^2$ is the particle function describing the scattering of an isolated particle, and $S(Q)$ describes interparticle effects.

Ellipsoids. The equations used here for asymmetric particles were those in ref 2, modified for multiple shells. The rationale for details of the interpretation is given in that reference and more extensively in ref 5.

As in previous studies of related composition,[1−5] we find that the models giving the best fit and the closest approximation to experimental absolute intensities are monodisperse oblate ellipsoids, with an outer shell penetrated by the continuous phase. When only the single components D_2O or $C_{16}D_{34}$ provide contrast, the fits are relatively indifferent to handling of the shell in the particle function, but when, as here, two or more components are deuterated in individual runs, detailed specification of the shells is necessary.

Several variations were tried; the results presented in detail here are for a core comprised of all the water in the composition and the K^+ counterions: shell 1, of uniform thickness, comprised of surfactant carboxylates and the hydroxyl groups of alcohols in the particle; shell 2, also of uniform thickness, containing the hydrocarbon of the particle alcohol and part of the surfactant hydrocarbon; shell 3, of the balance of the surfactant hydrocarbon; and the continuous phase, of hexadecane and the rest of the alcohol.

For the heptanol compositions, seven methylenes and one −CH═ of the oleate hydrocarbon were assigned to shell 2; for octanol, seven methylenes and −CH═CH− were included in shell 2.

In addition to the more detailed delineation of the shells, there is another significant difference from the model used in the D_2O contrasts of ref 1. There shell 1 was included in the core (there is relatively little contrast between the D_2O core and the shell groups), and the rest of the particle was combined in a single shell, comprised of surfactant and alcohol hydrocarbon plus penetrating continuous phase and shells of other particles. The amount of penetrating matter was that necessary to fill the rest of the noncore volume; the total particle volume was defined by the radius of the sphere of equivalent volume to that of the total ellipsoid, obtained in the least-squares fit. Least-squares values of this radius were influenced primarily by the interparticle structure function. The structure function, was computed by what was essentially a Percus−Yevick approach,[10] modified for penetration. Three parameters are involved: a distance of closest approach, which was the total radius; the volume fraction of the disperse phase; and a factor[11] between 0 and 1, multiplied by the volume fraction, to account for the penetration of the outer shell by continuous phase and other shells. The (single) particle function was relatively insensitive to total radius, because the contrast between the hydrocarbon in the shell and that in the continuous phase was low. With the higher contrasts here, however, the shell dimensions are no longer trivial in the particle function. Consequently, least-squares was no longer free to converge on a total-particle radius that was essentially a favorable distance of closest approach. The earlier assignment of a structure−function dimension of ellipsoids as the radius of a sphere of equivalent volume is no longer satisfactory. Specifically, besides poor fits, nonphysical parameters were encountered; the total radius sometimes gave volumes not large enough to accommodate all the material the other parameters put into the particles. These difficulties were overcome by using R_2 for the (interparticle) structure function only, and deriving the dimensions of the various shells in the (single) particle function from the particle composition, with the outermost shell 3 modeled as a compact layer of the oleate hydrocarbon not assigned to shell 2.

This procedure avoids adding another varied parameter, but the particle function here has a small inconsistency, in that penetration of the outermost shell is neglected. However, the lower volume of the shell is compensated by the higher contrast with the continuous phase, and the overall effect should be small.

The equations[2] for the particle function of an ellipsoid were those given by Hayter[12] and by Kotlarchyk and Chen.[13] The structure function was computed by the Mean Spherical Approximation (MSA) program of Hayter et al.,[14−16] with the

specification of a vanishingly small charge on the particles, which reduces the structure function essentially to Percus−Yevick. The geometrical and dimensional quantities varied in the least-squares fit were R_{core}, the radius of a sphere equivalent to the volume of the ellipsoidal core; R_2, here the MSA distance-of-closest-approach parameter of the structure function; the core axial ratio, *AR*, the ratio of the axis around which the ellipse is rotated to form the ellipsoid to the other axis (<1 for oblate, >1 for prolate); the penetration factor; and the number of moles alcohols/mole of surfactant in the particle, N^{shell}. These quantities are the same for all contrasts of a given stoichiometry. The number of surfactant molecules per particle, *AGG*, is given (volumes in this context in Å^3/molecule or ion or group) by

$$AGG = {}^4/_3\pi R_{core}{}^3/(N_w V_w + V_{K^+})$$

where N_w is the number of water molecules per mole of surfactant, V_w is the volume of a molecule of water, and V_{K^+} is the volume of K^+. The volume of shell 1 in Å^3 is *AGG*-($V_{carboxylate} + N^{shell}V_{-OH}$) or $AGG(34.3 + 17N^{shell})$. The volume of shell 2 is *AGG* times (the volume of surfactant hydrocarbon assigned to the shell for heptanol or octanol (see above) plus N^{shell} times the volume of hydrocarbon of the alcohol in question). The volume of shell 3 is *AGG* times the volume of the balance of surfactant hydrocarbon. From these shell volumes, the thicknesses of uniform shells and the volumes of the ellipsoids comprised of the core plus the successive ellipsoids are computed, and the axial ratios for these successive ellipsoids are also obtained. The scattering-length densities are computed for the core and shells from their isotopic compositions and volumes of the constituents. From these quantities, the particle function is calculated by numerical integration over all orientations of the ellipsoid with respect to the direction of the neutron beam by the equations in refs 12 and 13, modified for multiple shells.

A quantity, R_{tot}, the radius of a sphere of the same volume as the ellipsoid defined above, is also reported. The total volume of the particle, $({}^4/_3)\pi R_{tot}{}^3$, along with the concentration of particles (moles/liter of potassium oleate (KOleate) divided by *AGG*, converted to molecules/Å^3), determines the volume fraction of particles. Because the volume fraction is multiplied by the penetration factor in the computation of the structure functions, the neglect of the contribution of penetrating continuous phase to volume fraction is irrelevant.

Another quantity derived from the results, the carboxylate area, is computed by reversing the procedure in ref 1: from the area (in Å^2) of the core/shell 1 interface, the area occupied by alcohol ($AGG \times N^{shell} \times 20$ Å^2) is subtracted, and the difference is divided by *AGG* to give an estimate of the area occupied by the carboxylate headgroup of the surfactant.

From the (single) particle function, (interparticle) structure function, and particle concentration, the absolute intensity of coherent scattering is computed.[12,13] Two other quantities for each individual contrast are varied in the least-squares. A flat contribution to intensity, arising primarily from incoherent scattering, is added to the intensities, independent of *Q*. Because the calibration to convert experimental results to absolute intensities is good only to perhaps 20%, a constant factor *SCALE* is included in the least-squares; it is multiplied by the computed absolute intensity at each *Q*. This procedure avoids distortion of other parameters in trying to match computed intensities to experimental. If the calibration factor, the model, and the experimental results were all completely correct, the values of *SCALE* would be 1. Departures from unity are one test of the applicability of the model used, but those within 20% provide little information on the validity.

In carrying out the fits, we found it advantageous to obtain starting parameters R_{core}, *AR*, R_2 and the penetration factor by fitting only the D_2O and $C_{16}D_{34}$ with shell alcohol N^{shell} fixed at an intermediate value. The other three contrasts were then added to the set, and all parameters, including N^{shell}, were varied.

Polydisperse. A similar model with three shells was tested for a Schulz distribution of polydisperse spheres. Here, the approximation of using a structure function for spheres was not necessary, and R_2 applied both to the distance-of-closest-approach and to the total particle. The outermost shell therefore was comprised of residual surfactant hydrocarbon plus invading continuous phase and shells of other particles needed to fill the available volume. The equations were developed by Griffith et al.[17] and were modified for particles of three shells. In this model, the Schulz breadth parameter, *SZ*, was varied instead of an axial ratio.

Comparison of Computed and Experimental Patterns. Oblate Ellipsoids. The computed curves for oblate ellipsoids are given in Figures 1−3, and the parameters are listed in Table 2. The fits cannot be expected to match experiments as well as fits to patterns with only D_2O or $C_{16}D_{34}$ contrast, where essentially only one region is delineated. However, the curves for C8c and C7c do follow reasonably well the minima or inflections of the contrasts with shells, although in both cases, there is fine structure in the computed curves not seen in the experiments. The correspondence between experiment and computation is less satisfactory with C7C, but there is a general similarity.

Of the three compositions, the results with the octanol composition C8c seem best. The match of computed and experimental absolute intensities is good, *SCALE* values all being within 15% of unity. The least-squares fit criterion χ (the square root of the [(sum of the squares of weighted residuals)/(number of points − number of parameters + 1)]) is also lowest for this composition. However, although this quantity is useful in evaluating different models for a given set of contrasts, it is more limited in judging fits of different compositions, because it reflects the precision of the results.

The fits for C7c (Figure 2), although not as good, are satisfactory. The discrepancies at higher angles probably are caused by higher residual intensity from the smaller particles; the incoherent parameters were not constrained by a region of the pattern in which all other contributions were minor. With the exception of the $C_7D_{15}OH$-only contrast, values of *SCALE* were within experimental uncertainty. The relatively low intensities from the alcohol contrast perhaps make this parameter less well determined.

The fits were least satisfactory for C7C (Figure 3). Discrepancies at high *Q* and illogical values of the incoherent parameters (e.g., lower for D_2O than for $D_2O/C_{16}D_{34}$) probably arise in part from the even smaller particle sizes than with C7c. In addition, with C7C, the converged value of N^{shell} differed with the initial value used; if least-squares was started with a low value, N^{shell} ended up at 2.01 ± 0.04, instead of 3.59. The fit was about equal, and the other parameters were not greatly different. We report the set with 3.6 shell alcohols because its implied carboxylate headgroup area is more consistent with the other compositions. The lower scattering may explain some of the erratic matches of computed to experimental absolute intensities (*SCALE*s 0.5−1.6). However, these inconsistencies may indicate that the ellipsoidal model is a poorer approximation for this composition.

Values of R_{tot} and of the semimajor and semiminor axes of the total particle, as determined for the particle function, are also listed in Table 2. The values of the distance-of-closest-

TABLE 2: Fitting Parameters for Contrast Measurements of Alcohol Distribution: Oblate Ellipsoids

	C8c	C7c	C7C
MOLES			
KOleate	1	1	1
water	45	45	30
hexadecane	15	15	5.5
1-octanol	5.5		
1-heptanol		7.2	7.2
SCALE, ratio experimental to computed absolute intensities			
D_2O	0.870 ± 0.008	1.08 ± 0.01	1.12 ± 0.02
$C_{16}D_{34}$	0.85 ± 0.01	1.09 ± 0.02	0.75 ± 0.01
$D_2O/C_{16}D_{34}$	0.92 ± 0.03	0.99 ± 0.03	0.40 ± 0.02
$C_7D_{15}OH$ or $C_8D_{17}OH$	0.90 ± 0.07	1.6 ± 0.1	1.6 ± 0.2
$D_2O/C_{16}D_{34}/C_7D_{15}OH$ or $C_8D_{17}OH$	0.89 ± 0.02	0.84 ± 0.02	0.52 ± 0.02
INCOHERENT, $d\Sigma(Q)/d\Omega$, cm^{-1}			
D_2O	0.55 ± 0.02	0.86 ± 0.03	0.67 ± 0.05
$C_{16}D_{34}$	0.25 ± 0.02	0.67 ± 0.03	1.40 ± 0.04
$D_2O/C_{16}D_{34}$	0.45 ± 0.02	0.63 ± 0.04	1.45 ± 0.05
$C_7D_{15}OH$ or $C_8D_{17}OH$	1.10 ± 0.03	1.12 ± 0.03	1.19 ± 0.07
$D_2O/C_{16}D_{34}/C_7D_{15}OH$ or $C_8D_{17}OH$	0.136 ± 0.004	0.122 ± 0.008	0.24 ± 0.01
R_{core}, Å	50.4 ± 0.1	45.8 ± 0.2	26.6 ± 0.2
R_2, Å	55.3 ± 0.3	51.4 ± 0.4	34.8 ± 0.2
axial ratio, *AR*	0.481 ± 0.004	0.468 ± 0.005	0.397 ± 0.007
penetration factor	0.885 ± 0.009	0.86 ± 0.01	0.66 ± 0.01
particle alcohols/KOl	2.69 ± 0.06	2.76 ± 0.06	3.59 ± 0.05
IMPLIED QUANTITIES			
R_{tot}, Å	62.2	56.3	35.9
ellipsoid, semimajor axis	75.4	68.8	44.8
ellipsoid, semiminor axis	42.2	37.6	23.0
aggregation no., *AGG*	385−398	294−299	85−86
carboxylate area, $Å^2$	35−38	43−45	48−50
X	5.1	6.9	5.7

TABLE 3: Fitting Parameters for Contrast Measurements of Alcohol Distribution: Prolate Ellipsoids

	C8c	C7c	C7C
MOLES			
KOleate	1	1	1
water	45	45	30
hexadecane	15	15	5.5
1-octanol	5.5		
1-heptanol		7.2	7.2
SCALE, ratio experimental to computed absolute intensities			
D_2O	0.89 ± 0.02	1.09 ± 0.02	0.99 ± 0.02
$C_{16}D_{34}$	0.87 ± 0.02	1.10 ± 0.03	0.94 ± 0.02
$D_2O/C_{16}D_{34}$	0.86 ± 0.04	0.91 ± 0.04	0.97 ± 0.07
$C_7D_{15}OH$ or $C_8D_{17}OH$	0.82 ± 0.09	1.2 ± 0.1	1.4 ± 0.1
$D_2O/C_{16}D_{34}/C_7D_{15}OH$ or $C_8D_{17}OH$	0.87 ± 0.03	0.85 ± 0.02	0.38 ± 0.02
INCOHERENT, $d\Sigma(Q)/d\Omega$, cm^{-1}			
D_2O	0.57 ± 0.04	0.92 ± 0.04	1.00 ± 0.04
$C_{16}D_{34}$	0.27 ± 0.03	0.71 ± 0.04	1.56 ± 0.04
$D_2O/C_{16}D_{34}$	0.48 ± 0.04	0.63 ± 0.05	1.37 ± 0.06
$C_7D_{15}OH$ or $C_8D_{17}OH$	1.11 ± 0.05	1.18 ± 0.04	1.49 ± 0.04
$D_2O/C_{16}D_{34}/C_7D_{15}OH$ or $C_8D_{17}OH$	0.137 ± 0.006	0.122 ± 0.008	0.12 ± 0.01
R_{core}, Å	56 ± 1	51 ± 1	26.6 ± 0.5
R_2, Å	56.3 ± 0.7	52.8 ± 0.6	35.4 ± 0.2
axial ratio, *AR*	2.9 ± 0.2	2.8 ± 0.2	2.1 ± 0.1
penetration factor	1.03 ± 0.04	0.99 ± 0.04	0.70 ± 0.03
particle alcohols/KOl	2.7 ± 0.1	2.88 ± 0.09	2.02 ± 0.04
IMPLIED QUANTITIES			
R_{tot}, Å	69.7	62.5	33.9
ellipsoid, semimajor axis	126.3	112.4	50.0
ellipsoid, semiminor axis	51.6	46.7	27.9
aggregation no., *AGG*	541−555	398−406	85−88
carboxylate area, $Å^2$	30−33	45−47	70−73
X	9.5	8.6	5.9

approach parameter, R_2, in each case fall between the semiaxes, as one would expect; R_2 is also consistently less than R_{tot}.

The range of aggregation number and carboxylate area values arise from the minor differences in mol of water/mol of KOleate in the experimental compositions for the different contrasts. By the computational procedure, the core volume, from R_{core}, is the same for all of a given composition, so these differences in stoichiometry result in differences in *AGG*. There was a corresponding small spread in the listed values of R_{tot} and the ellipsoidal axes, and the values listed in the tables are averages.

For all three compositions, N^{shell} was greater than we estimated from core-area arguments.[1] We shall discuss this later.

Prolate Ellipsoids. Table 3 summarizes the parameters for fits to prolate ellipsoids. Here, in contrast to our earlier experience with only D_2O contrasts, the computed absolute

TABLE 4: Fitting Parameters for Contrast Measurements of Alcohol Distribution: Polydisperse Spheres

	C8c	C7c	C7C
MOLES			
KOleate	1	1	1
water	45	45	30
hexadecane	15	15	5.5
1-octanol	5.5		
1-heptanol		7.2	7.2
SCALE, ratio experimental to computed absolute intensities			
D_2O	0.69 ± 0.03	0.74 ± 0.01	0.82 ± 0.01
$C_{16}D_{34}$	0.64 ± 0.03	0.61 ± 0.01	0.713 ± 0.009
$D_2O/C_{16}D_{34}$	0.11 ± 0.01	0.27 ± 0.03	0.084 ± 0.004
$C_7D_{15}OH$ or $C_8D_{17}OH$	0.032 ± 0.004	0.015 ± 0.001	0.062 ± 0.006
$D_2O/C_{16}D_{34}/C_7D_{15}OH$ or $C_8D_{17}OH$	0.77 ± 0.09	1.03 ± 0.07	0.24 ± 0.01
INCOHERENT, $d\Sigma(Q)/d\Omega$, cm^{-1}			
D_2O	0.61 ± 0.05	0.93 ± 0.04	1.06 ± 0.04
$C_{16}D_{34}$	0.29 ± 0.04	0.68 ± 0.05	1.49 ± 0.04
$D_2O/C_{16}D_{34}$	0.94 ± 0.04	0.95 ± 0.07	1.64 ± 0.04
$C_7D_{15}OH$ or $C_8D_{17}OH$	1.47 ± 0.05	1.58 ± 0.03	1.78 ± 0.02
$D_2O/C_{16}D_{34}/C_7D_{15}OH$ or $C_8D_{17}OH$	0.16 ± 0.01	0.15 ± 0.01	0.24 ± 0.01
R_{core}, Å	41.9 ± 0.7	36.5 ± 0.3	22.5 ± 0.3
R_2, Å	55.1 ± 0.6	48.59 ± 0.05	36.9 ± 0.2
Schulz breadth, SZ	35± 3	29 ± 2	84 ± 9
penetration factor	0.75 ± 0.05	0.68 ± 0.03	0.39 ± 0.01
particle alcohols/KOl	2.2 ± 0.4	5.7 ± 0.2	1.6 ± 0.1
IMPLIED QUANTITIES			
aggregation no., *AGG*	239−247	163−166	53−54
carboxylate area, $Å^2$	47−50	(−9)-(−11)	88−89
X	11.9	8.6	5.2

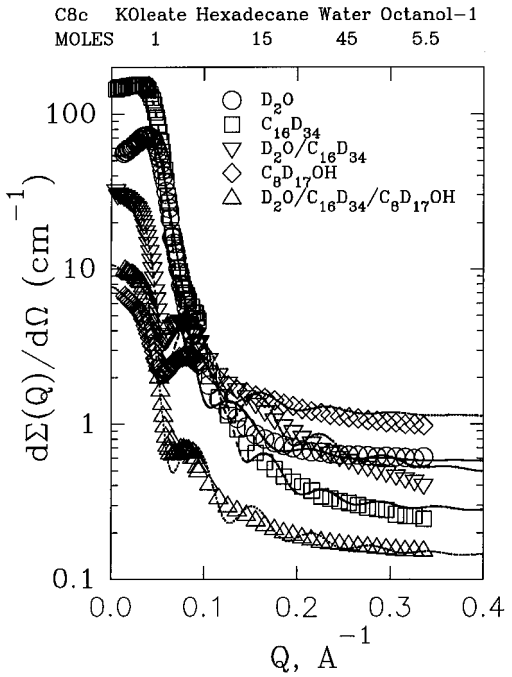

Figure 4. Prolate ellipsoidal model, C8c. Symbols, experimental points, indicate deuterated components. Parameters of computed curves in Table 3.

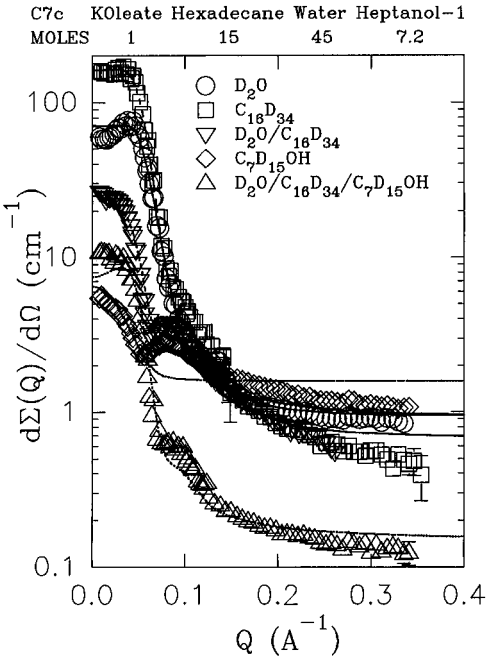

Figure 5. Polydisperse-spheres model, C7c. Symbols, experimental points, indicate deuterated components. Parameters of computed curves in Table 4.

intensities were about as satisfactory as with oblate geometry. However, as the *X* values indicate, the fits were poorer, substantially so for C8c and C7c. Figure 4 illustrates this for C8c. There is considerable fine structure in the computed curves not seen in the experiments. The values of carboxylate areas are more erratic than for oblate ellipsoids.

Polydisperse Spheres. The parameters obtained by least-squares of the polydisperse-spheres model are summarized in Table 4. The radii and *AGG* listed are number averages. Agreements between computed and experimental patterns were much poorer for C8c and C7c than for oblate ellipsoids. The X for the relatively unstructured pattern of C7C was a little smaller for polydisperse than for oblate ellipsoids, but the agreement in the low-*Q* region of ellipsoids, probably a better test of the competing models, was visually better for oblate. The polydisperse parameters were erratic, particularly the absolute-intensity *SCALE*s, and the carboxylate areas computed for C7c and C7C were not plausible.

The polydisperse fit for C7c is shown in Figure 5. The correspondence at low *Q* is seen to be poor, and the fine structure around $Q = 0.1$ is largely washed out in the computed curves for the compositions with contrasting shells. Deviations with C8c were similar and even more marked.

Other. One might argue that the K^+ counterions would tend to localize in the first shell, near the carboxylates, rather than to be distributed uniformly through the core. Because of the

high dielectric constant of water, we are not dealing with a Faraday cage. We tested for oblate ellipsoids putting the counterions in the shell. The proximity of counterions to negatively charged carboxylate groups probably limits the electrostriction of hydrated water, which is reflected in the volumes used, and we attempted to allow for this effect. For the volume of KCO_2^- we estimated 52 Å^3, by adjusting the 40 Å^3 total of potassium ion plus carboxylate for the difference[18] between the volume of the un-ionized carboxylate and H^+ plus $-CO_2^-$. The fits and parameters were insignificantly different from those obtained with K^+ distributed in the core. This is not surprising; the thickness of the first shell is less than an angstrom, and differences in the two models are probably undetectable with the resolution of our experiments.

Discussion

We conclude, as in previous studies, that the oblate-ellipsoidal model represents the experimental results better than prolate ellipsoids or polydisperse spheres.

Our preference for oblate ellipsoids as the closest description of the disperse-phase particles in the potassium oleate water/oil microemulsions is based on fits to SANS patterns and the physical reasonableness of the parameters of the models used to obtain the fits. The plausibility of such a distribution from a microscopic and thermodynamic point of view was discussed in earlier papers, particularly in ref 5. The cosurfactant headgroup presumably increases stability by increasing the spacing between the charged carboxylate groups. The composition, shape, and distribution of the particles result from a complex array of factors. Size of the water core is primarily a function of water/surfactant ratio,[5] with the particle alcohol reinforcing the surfactant, i.e., decreasing the effective water/surfactant ratio, reflected in the size of the cores.[1] Increasing the alcohol concentration in the system increases the number of alcohols/particle, but the fraction of alcohol distributed in the particle decreases.[1] The asymmetry of the core presumably arises from the need for more surface area to accommodate the headgroups than spheres provide; the energetic penalty of increased curvature is balanced against the lower free energy of an alcohol in the particle vs in the continuous phase.

The ellipsoidal models we used are for monodisperse systems. Although in our opinion, analysis of the results convincingly rules out polydisperse spheres (at least with a Schulz distribution), it does not exclude a distribution of sizes in the ellipsoids, narrow enough not to obscure the basic features of the patterns reflecting asymmetry. It could be argued that the fine structure in the computed curves not matched in the experimental patterns (particularly at high Q) indicates some polydispersity. However, these deviations generally occur in regions of low intensity, and, in view of smearing, we believe such an attribution is premature.

In that regard, our preference for oblate over prolate geometry might be questioned here. Although the least-squares fit parameters were considerably better for oblate than for prolate, the differences appear to arise (Figure 4) from greater fine structure in the computed curves for prolates, although they oscillate rather faithfully about the experimental patterns. If smearing is greater than we think, prolates might be an option. The smaller spread of carboxylate areas derived from the oblate model than from prolate supports our choice of oblate here.

Our confidence in our conclusions is fairly high with C8c and C7c; with C7C, none of the models gave a very satisfactory explanation, although the oblate-ellipsoidal was at least marginally better. Some of the difficulty with C7C, as well as imperfections of the fits with C8c and C7c, comes from the slight differences in mole ratios of the various compositions in the sets. However it seems probable that more of the difficulty arises from the resolution of the experiments. An earlier set of patterns measured with the C7C composition had even less definition in the compositons having contrasts between core and continuous phase vs shells than those in Figure 3. Attempts to fit these to any model by least-squares were unsatisfactory; the computed curves bore little relation to the experiments, and the parameters were not plausible and, at times, unphysical. The results in Figure 3 were obtained with smaller slits and consequently are less smeared.

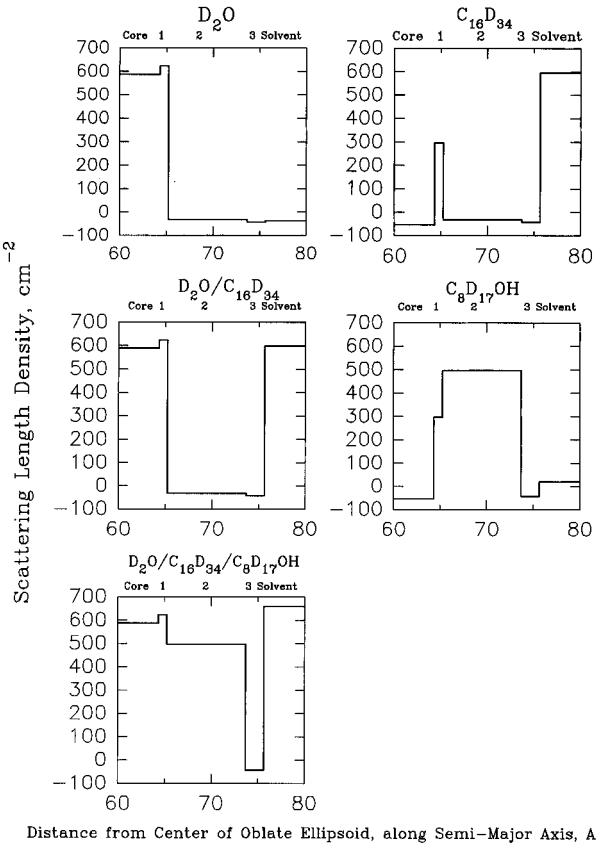

Figure 6. Contrasts for C8c, oblate ellipsoidal model. Core; shells 1, 2, 3; continuous phase (solvent).

Clearly, in studies of this type good resolution is desirable. Modifications of the High Flux Isotope Reactor under consideration would greatly decrease smearing; higher neutron fluxes would allow use of smaller slits, and a chopper would be feasible to sort out the spread of neutron energies by time-of-flight. Also, a cold source would extend downward the range of Q available. It is hoped that the relatively modest funds needed for these advances can be found.

In any case, the vast difference in patterns for the same chemical compositions but different isotope labels seen here illustrates again the great leverage small-angle neutron scattering provides in delineating structures in the nanometer and higher range. Figure 6 illustrates for the fit by the oblate-ellipsoid model to C8c the contrasts between the various regions for the different isotope labels. With only D_2O or hexadecane deuterated, the pattern derives mainly from the contrast between core and the rest or between total particle and continuous phase. With the others, contrasts between one or more of the shells and the rest determine the patterns. Simultaneous fits to all constrain greatly the range of possible models.

The distribution of alcohols in the particles measured relatively directly here by contrasts is higher than estimated by core area arguments in ref 1. The carboxylate areas derived from the present results are consequently smaller than the 60

Å^2 used earlier for estimation of alcohol partition. However, for the reasons discussed in the Introduction, such differences are not surprising. In future estimates of alcohol distributions from D_2O-only contrasts, the results here suggest that a smaller value, perhaps 45 Å^2, for carboxylate area would be better. There is also of course uncertainty in the 20 Å^2 assumed for the alcoholic headgroup, and the core-area procedure can be expected to give only a rough approximation of alcohol distribution.

With respect to values of other parameters reported here, the particle sizes for C8c and C7c are somewhat larger (about 5% in R_{core}) than computed for the D_2O-only experiments of ref 1, and for C7C, about 6% smaller. With C8c and C7c, for which oblate ellipsoids seemed a good model, the numbers from the complete set of contrasts are probably better than from a single contrast.

Acknowledgment. The research was supported (A.L.C., W.L.G., J.S.J.) by the Division of Energy Efficiency and Renewable Energy, and (DC-M) by the Division of Material Sciences, U.S. Department of Energy, under Contract DE-AC05-96OR22464 with Oak Ridge National Laboratory, managed by Lockheed Martin Energy Research Corporation. R.T. acknowledges financial support from the Italian National Research Council and from the Ministero dell' Università e della Ricerca Scientifica e Tecnologica. We thank George Wignall of the Solid State Division, Oak Ridge National Laboratory, for use of facilities and for advice in their operation. We are indebted to Elijah Johnson of the Chemical and Analytical Sciences Division for reading the paper and for helpful suggestions.

References and Notes

(1) Caponetti, E.; Lizzio, A.; Triolo, R.; Griffith, W. L.; Johnson, J. S., Jr. *Langmuir* **1992**, *8*, 1554.
(2) Caponetti, E.; Magid, L. J.; Hayter, J. B.; Johnson, J. S., Jr. *Langmuir* **1986**, *2*, 722.
(3) Caponetti, E.; Griffith, W. L.; Johnson, J. S., Jr.; Triolo, R.; Compere, A. L. *Langmuir* **1988**, *4*, 606.
(4) Caponetti, E.; Lizzio, A.; Triolo, R.; Compere, A. L.; Griffith, W. L.; Johnson, J. S., Jr. *Langmuir* **1989**, *5*, 357.
(5) Caponetti, E.; Lizzio, A.; Triolo, R. *Langmuir* **1990**, *6*, 1628.
(6) Scatchard, G. *Equilibrium in Solutions; Surface and Colloid Chemistry*; Harvard University Press: Cambridge, MA, 1976; p 239.
(7) Høiland, H. *Acta Chem. Scand*. **1974**. *A28*, 699.
(8) Ho, P. C.; Triolo, R.; Johnson, J. S., Jr. *J. Phys. Chem*. **1995**, *99*, 9581.
(9) Kostorz, G.; Lovesey, S. W. *Treatise on Materials Science and Technology*; Academic Press: New York, 1979; Vol. 15, pp 230−231.
(10) Ashcroft, N. W.; Lekner, J. *Phys. Rev*. **1966**, *145*, 83.
(11) Blum, L.; Stell, G. *J. Chem. Phys*. **1979**, *71*, 42; **1980**, *72*, 2212.
(12) Hayter, J. B. In *Physics of Amphiphiles: Micelles Vesicles, and Microemulsions*; Degiorgio, V., Corti, M., Eds.; North-Holland: Amsterdam, 1985; p 59.
(13) Kotlarchyk, M.; Chen, S.-H. *J. Chem. Phys*. **1983**, *79*, 2461.
(14) Hayter, J. B.; Penfold, J. *Mol. Phys*. **1981**, *42*, 109.
(15) Hansen, J.-P.; Hayter, J. B. *Mol. Phys*. **1982**, *46*, 651.
(16) Hayter, J. B.; Penfold, J. *J. Chem. Soc., Faraday Trans. 1* **1981**, *77*, 1851.
(17) Griffith, W. L.; Triolo, R.; Compere, A. L. *Phys. Rev. A* **1986**, *33*, 2197; **1987**, *35*, 2200.
(18) Millero, F. J. In *Water and Aqueous Solutions*; Horne, R. A., Ed.; Wiley-Interscience: New York, 1972; Chapter 13, p 519.